




# Possible measure of soil factors in the Italian seismic code

Dario Albarello<sup>1,2</sup> · Enrico Paolucci<sup>3</sup> 

Received: 13 April 2024 / Accepted: 17 September 2024  
© The Author(s) 2024

## Abstract

The Italian seismic code provides a simplified approach to account for the effect of local seismostratigraphical configuration on the expected ground motion. This approach, common with other seismic codes, provides specific ‘soil factors’ as a function of a set of reference subsoil conditions (soil classes): these factors are considered in 1D subsoil configurations to modify the uniform probability hazard spectrum deduced from probabilistic seismic hazard at reference soil conditions. It is inferred that, to provide a coherent management of uncertainty affecting the response spectrum to be used for the design, the contribution of uncertainty affecting soil factors must be carefully considered to avoid biases in the hazard evaluation. In the present study, variability of soil factors representative of each soil class has been explored by numerical simulation relative to many seismostratigraphical configurations inferred from seismic microzonation studies available in Italy relative to 1689 municipalities. This analysis shows that variability of soil factors is of the same order of magnitude of variability affecting reference response spectra, which implies that the former cannot be neglected as presently happens in the common practice. It is also shown that neglecting this contribution can lead to underestimate the impact of subsoil configuration on the regularized response spectrum provided by the norm, in particular, in the short period range.

**Keywords** Seismic site amplification · Italian seismic code · Soil factors · Local seismic response analyses · Seismic microzonation

---

✉ Enrico Paolucci  
enrico.paolucci3@unibo.it

<sup>1</sup> Department of Physical, Earth and Environmental Sciences, University of Siena, Siena, Italy

<sup>2</sup> Consiglio Nazionale delle Ricerche, Istituto di Geologia Ambientale e Geoingegneria, Rome, Italy

<sup>3</sup> Department of Physics and Astronomy, University of Bologna, Bologna, Italy

# 1 Introduction

Current seismic codes establish that the design of earthquake resistant structures requires an estimate of the expected ground shaking at the site of interest in the form of acceleration response spectra. Due to the lack of knowledge concerning the faulting and long-range ( $> 10^3$  m) energy propagation processes, many possible scenarios are considered as possible, whose respective likelihood is assessed by considering probabilistic Ground Motion Prediction Equations (GMPEs). These equations allow computing the exceedance probability associated to response spectrum ordinates, as function of a small number of parameters generally representative of the distance from the source and of released energy. The GMPEs are determined empirically by the statistical analysis of available accelerometric registrations for the region of interest by considering a conventional subsoil condition (generally a rigid subsoil with flat morphology). When the design concerns other subsoil configurations, the reference response spectrum must be modified as function of the small-scale ( $< 10^3$  m) morpho-stratigraphical configuration. In these cases, specific studies are required (local seismic response analysis) to account for these effects based on suitable numerical procedures fed by site specific field and laboratory data. These studies may be expensive and thus most building codes also provide abacuses to estimate the effect of non-reference subsoil conditions for a small set of simple 1D stratigraphical (soil classes) and 2D morphological configurations (topographic classes) easily identifiable thanks to appropriate proxies: for these configurations, specific parameters (soil factors) are determined to adapt the reference response spectrum to the site situation. As an example, soil factors of this kind are provided in the Italian seismic code (NTC18, 2018) with the explicit indication (see Sect. 7.11.3 of the code) that these cannot be used when lateral 2D or 3D heterogeneities exist in the considered subsoil configuration which make inappropriate any 1D model.

These factors are determined based on empirical or numerical approaches. In the first case, statistical analysis of accelerometric records at the different soil classes is performed (e.g., Rey et al. 2002; Paolucci et al. 2021); main drawbacks and advantages of this approach are largely discussed in the literature (see Paolucci et al. 2021 and references therein). In the second approach, the soil factors are determined by the considering large sets of subsoil profiles feeding numerical simulations (e.g., Andreotti et al. 2018; Aimar et al. 2020). The main advantage of the numerical approach is the possibility to simulate an arbitrary high number of strictly 1D seismostratigraphical configurations. The main limitation of this approach relies on the appropriateness of the computational model used to represent the propagation process and the representativeness of the considered configurations with respect to the existing ones. Where the former problem can be overcome by considering computationally onerous procedures, the latter is addressed by selecting a set of configurations assumed to be representative of most diffuse situations. Therefore, the results of the simulations will be applicable only under the conditions accounted in the computational model. More in general, empirical, and numerical approaches could be seen as complementary (Paolucci et al. 2021).

The following discussion focuses on 1D soil factors implemented in the current Italian seismic code (NTC18, 2018). Two aspects will be of main concern. First, the procedure to fit the reference response spectrum to the specific soil class is considered and possible drawbacks enlightened. Then, outcomes of new set of numerical simulations are presented, which accounts for the dataset made available by 1689 seismic microzonation studies rel-

ative to as many municipalities and conducted following a standard approach (SM-WG, 2008) in the last 10 years in Italy. Analyses of the same type have already been attempted in the past (Andreotti et al. 2018; Paolucci et al. 2021) starting from random variations of theoretical (Andreotti et al. 2018) or experimental (Paolucci et al. 2021) velocity profiles, but still in relatively small numbers compared to the variety of situations present on the Italian territory. It is worth to note that the following discussion will not concern effectiveness of the subsoil classification adopted in the Italian seismic code, which should deserve specific analyses not performed here.

## 2 Soil factors in Italian seismic code (NTC18)

No public documentation exists regarding how the soil factors were determined for the soil classes adopted in the Italian seismic code (Table 1).

We assume that an empirical approach like the one described Rey et al. (2002) was adopted. Based on the analysis of several accelerometric records, soil factor  $Sf_*$  as a function of the vibration period  $T$  at the generic ‘\*’ subsoil condition is determined by the ratio.

$$Sf_*(T) = \frac{Sa_*(T)}{Sa_{A(T)}}, \tag{1}$$

where  $Sa_A$  represents the acceleration response spectrum for the horizontal component of the ground motion relative to the reference subsoil configuration (under planar morphology conditions) and  $Sa_*$  represents the ordinate of the acceleration response spectrum for the horizontal component at the top of the considered the subsoil configuration other than the reference subsoil. From the population of values determined for each soil class and accelerometric registration, an average value  $\overline{Sf}_*(T)$  is extracted and considered as reference for the abacus in the code. Since the norm operates on standardized response spectra, the soil factors are reparametrized by considering two site specific values ( $S_S$  and  $C_c$  in NTC18; for details, see, e.g., Andreotti et al. 2018) which allows to adapt the regularized reference response spectrum to the site conditions (when these fit the respective soil class).

**Table 1** Description of soil classes considered in the current Italian seismic code (NTC18).  $V_{s_{eq}}$  indicated the harmonic average of shear wave velocity ( $v_s$ ) values down to seismic bedrock ( $v_s \geq 800$  m/s) when is shallower than 30 m and to 30 m in the other cases

Class	Description	$V_{s_{eq}}$
A	Outcropping rock or hard soil, including at most 3 m of weaker material at the surface	> 800 m/s
B	Soft rock or very dense cohesionless soil or very stiff cohesive soils characterized by gradual increase of mechanical properties with depth	360–800 m/s
C	Medium-dense cohesionless soil or medium-stiff cohesive soils, more than 30 m in thickness, characterized by gradual increase of mechanical properties with depth	180–360 m/s
D	Deposits of loose cohesionless soil or of soft cohesive soil, more than 30 m in thickness, characterized by gradual increase of mechanical properties with depth	100–180 m/s
E	Soils of class C or D up to 30 m in thickness underlain by stiffer material with $V_s$ , > 800 m/s	100–360 m/s

It worth to note that because the concept of ‘gradual increase of mechanical properties’ is coarsely defined, this condition is generally ignored by practitioners

A different integral parameterization accounting for site effects has been adopted by Italian Guidelines for Seismic Microzonation (IGSM) (SM-WG, 2008), where Amplification Factors relative to the generic ‘\*’ soil condition ( $AF_*$ ) are considered by means of the relationship

$$AF_*(T_1, T_2) = \frac{\int_{T_1}^{T_2} Sa_* dT}{\int_{T_1}^{T_2} Sa_A dT}, \tag{2}$$

where  $T_1$  and  $T_2$  are the extremes of the considered interval of periods (in the following, in sake of simplicity, the dependance on  $T_1$  and  $T_2$  will be omitted). According to IGSM, three reference intervals are defined regarding the vibration periods of buildings: 0.1–0.5 s, 0.4–0.8 s, 0.7–1.1 s (Moscatelli et al. 2020; Pergalani et al. 2020).

By considering the soil factors, the site-specific response spectrum can be determined.

Before proceeding, it is appropriate to discuss some formal aspects that have a significant impact in the implementation of soil factors in the norm. If the aim of the norm were computing a mean response spectrum, one could coherently state that.

$$\overline{Sa_*} = \overline{Sf_*} \overline{Sa_A} \tag{3}$$

where the horizontal bar refers to the average values of the considered parameters (the dependance on the period  $T$  has been omitted for simplicity). However, this is not the case of the Italian seismic code. In fact, the aim of the code is providing a conservative estimate of the seismic load accounting for the probabilistic character of the reference hazard estimate. This is performed by considering a Uniform Hazard Spectrum (UHS), whose spectral ordinates are characterized by a fixed exceedance probability. To preserve this property of the spectrum, variability of soil factors around the average should be accounted to avoid a significant underestimate of the seismic response at the non-reference site. To show this point, one can proceed as follows.

For consistency with the probabilistic character of hazard estimates, the spectral ordinate at the reference subsoil conditions  $Sa_A$  should be considered as a random variable resulting from the propagation of inherent uncertainties within the seismic hazard estimation procedure. For simplicity, it can be assumed that the variable  $Sa_A$  is characterized by a log-normal distribution with probability density  $p(Sa_A)$  given by the relation

$$p(\ln Sa_A) = \frac{1}{\sqrt{2\pi \sigma^2 \ln Sa_A}} e^{-\frac{(\ln Sa_A - \mu \ln Sa_A)^2}{2\sigma^2 \ln Sa_A}}, \tag{4}$$

where  $\mu$  and  $\sigma^2$  represent the mean and the variance respectively. The validity of this assumption can be easily assessed from the UHS provided by the reference hazard model (an example in Appendix 1).

Reasonably, the soil factor  $Sf_*$  can also be considered as a random variable characterized by a log-normal distribution and thus associated with a probability density

$$p(\ln Sf_*) = \frac{1}{\sqrt{2\pi} \sigma_{\ln Sf_*}^2} e^{-\frac{(\ln Sa - \mu_{\ln Sf_*})^2}{2\sigma_{\ln Sf_*}^2}} \tag{5}$$

Then, the spectral ordinate  $Sa_A$  on soil class A and  $Sf_*$  characterized by an exceedance probability  $\alpha$  will be respectively given by

$$\ln Sa_A(\alpha) = \mu_{\ln Sa_A} + k\sigma_{\ln Sa_A} \tag{6}$$

and,

$$\ln Sf_*(\alpha) = \mu_{\ln Sf_*} + k\sigma_{\ln Sf_*}, \tag{7}$$

where  $k = \mathbb{N}^{-1}(\alpha)$  and where  $\mathbb{N}$  is the standardized normal probability distribution. By the properties of the log-normal distribution, one has

$$\ln Sa_*(\alpha) = \ln Sa_A(\alpha) + \ln Sf_*(\alpha) = \mu_{\ln Sa_A} + \mu_{\ln Sf_*} + k\sqrt{\sigma_{\ln Sf_*}^2 + \sigma_{\ln Sa_A}^2 + 2cov(\ln Sf_*, \ln Sa_A)}. \tag{8}$$

However, if one discards variability of site factors (as commonly done in current practice) one has

$$Sa_*(\alpha) = Sf_*(\alpha) Sa_A(\alpha) \tag{9}$$

or,

$$\ln Sa_*(\alpha) = \mu_{\ln Sf_*} + \mu_{\ln Sa_A} + k\sigma_{\ln Sa_A} \tag{10}$$

One can see that this position provides a clear underestimate of the spectral ordinate, since

$$\sqrt{\sigma_{\ln Sf_*}^2 + \sigma_{\ln Sa_A}^2 + 2cov(\ln Sf_*, \ln Sa_A)} > \sigma_{\ln Sa_A} \tag{11}$$

Thus, to obtain an unbiased estimation of  $Sa_*(\alpha)$  it is necessary to jointly estimate  $\sigma_{\ln Sf_*}^2$  and  $\sigma_{\ln Sa_A}^2$ . Note that in the presence of nonlinear behavior of subsoil materials, which implies the dependence of  $Sa_A$  and  $Sf_*$  on PGA (e.g., Andreotti et al. 2018), the covariance term cannot be considered zero in principle.

### 3 The statistical characterization of the stochastic variable $Sf_*$ by numerical simulations

#### 3.1 The database

The first phase of the study aimed to establish a database that collect the outcomes of seismic microzonation studies available at the national scale and developed according to IGSM. These studies aim to characterize from a seismic point of view the urbanized areas of the national territory at the scale of the individual municipality. Based on the available geological, geotechnical, and geophysical information, the so-called Seismically Homogeneous Microzones (SHMs; e.g., Albarello 2017; Moscatelli et al. 2020) are identified by distinguishing SHMs subject to ground motion amplification phenomena (stable areas) and areas that may be subject to permanent deformation during the event (unstable areas). As for stable areas, each SHM is associated with a representative stratigraphic column in terms of a succession of Geological/Technical Units (GTUs) organized in the form of horizontal plane homogeneous layers. Each layer is associated with a range of thickness values according to the available information and the level of lateral heterogeneity present within the SHM. Based on this same information, a range of shear wave velocity ( $V_s$ ) values compatible with the observations is also associated with each layer (see, e.g., Pieruccini et al. 2022). These data were collected in the National Seismic Microzonation Database developed by the Institute of Environmental Geology and Geoengineering of the National Research Council (CNR-IGAG) on behalf of the Italian Department of Civil Protection (<https://www.webms.it/>) along with the information used to determine the SHMs (geognostic surveys, laboratory tests, borehole and surface seismic tests, etc.). This massive information was used for a statistical analysis that allowed the characterization of GTUs in terms of mean value, variance and covariance of  $V_s$  values, density, and shear modulus decay and damping curves as a function of depth (Romagnoli et al. 2022; Gaudiosi et al. 2023).

As a whole, the data collected covered 1689 municipalities with a total of 13,806 SHMs; their spatial distribution over the Italian territory and the Italian Seismic Hazard Map (Meletti et al. 2006) is shown in Fig. 1. This database constitutes the basis of the analyzes carried out and discussed below.

#### 3.2 Numerical modeling

Like the work of Andreotti et al. (2018) and Paolucci et al. (2021), local seismic response analyses related to the considered SHM were conducted using a 1D equivalent linear approach (Kramer 1996). Although this approach can be considered only approximate and has some limitations compared to more advanced forms of modeling (Yoshida et al. 2002; Kausel and Assimaki 2002; Kaklamanos et al. 2013, 2015; Andreotti and Calvi 2021), it remains the most widely used in professional practice also because of its greater robustness in terms of numerical convergence to the final solution. The computational code used is the one described by Acunzo et al. (2024), which implements the same direct modeling procedure implemented in the STRATA code (Kottke and Rathje 2008). The main advantage with respect to the latter code rely on the different randomization procedures considered to explore the effect of uncertainties related to the seismostratigraphic characterization of the considered column. This element plays a key role given the different amount of informa-

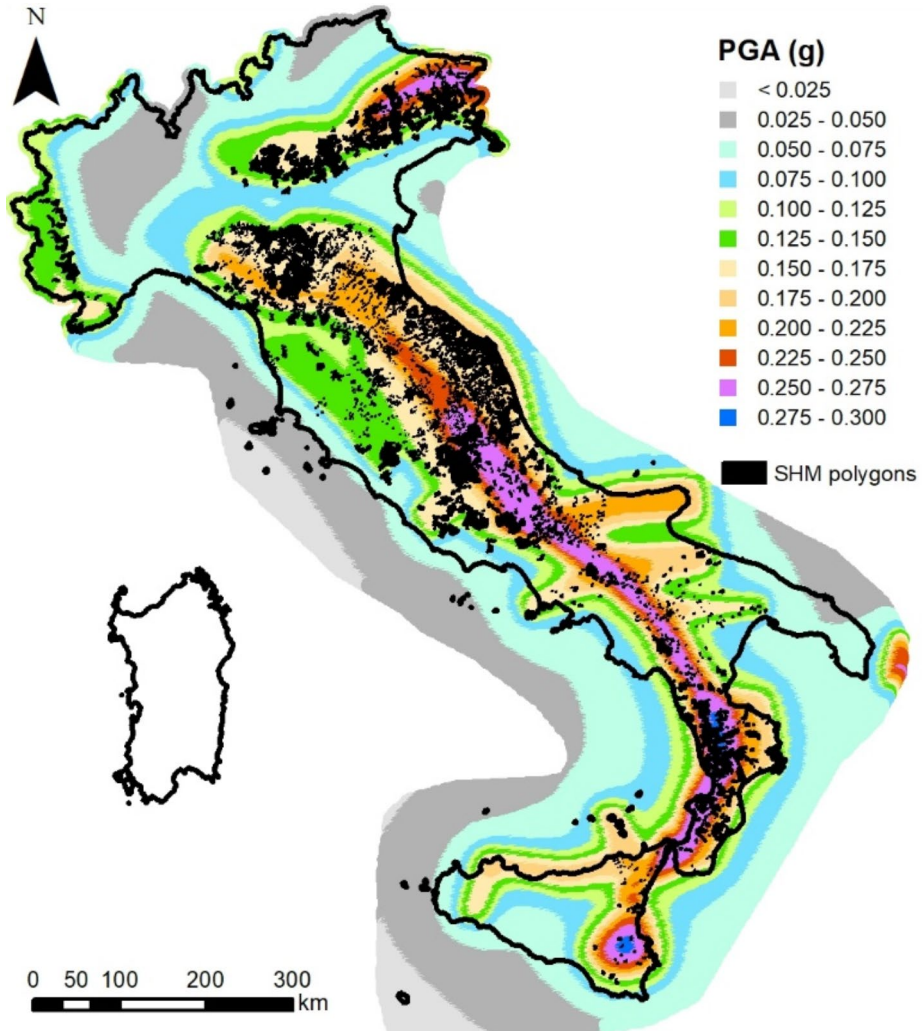


**Fig. 1** Distribution of the considered Seismically Homogeneous Microzones (SHMs; black polygons) over to Italian Seismic Hazard Map (Meletti et al. 2006). The colors refer to the Peak Ground Acceleration (PGA) classes (expressed as a fraction of the gravity acceleration  $g$ ) relative to an exceedance probability of 10% in 50 years

tion available for the situations analyzed. These uncertainties relate to two main aspects: mechanical characterization of the layer (thickness and GTU of the individual layer, the  $V_s$  values and the characteristic shear modulus decay and damping curves) and the depth of the seismic bedrock ( $H$ ) where the input ground motion relative to outcropping reference conditions must be applied. In general, in seismic microzonation studies, available data are generally able to set upper and lower limits of layer thickness and depth of the seismic bedrock. One or more GTU can be selected and, for each of them, a range of possible shear modulus decay and damping curves are considered as possible. To account for this uncertainty the following procedure has been followed for each SHM.

At first, a set of 100 seismostratigraphic columns is generated. Each column is defined as a stack of layers each characterized by a thickness and possible GTUs. The thickness of each layer and the relevant GTU are randomly extracted from a uniform distribution within the limits set by the original study. The resulting column is then discretized into 1 m-thick strata by assigning to each stratum a  $V_s$  value. When not uniquely determined in the original study, this value is chosen by a random extraction from a log-normal distribution, whose mean and variance values depend on depth and GTU by the empirical relationships determined by Romagnoli et al. (2022). The extracted values are constrained within the maximum and minimum limits set in the original study and conditioned by the value determined in the immediately shallower layer based on the correlation relationships also determined by Romagnoli et al. (2022). Shear modulus and damping decay curves are then associated with each layer as a function of GTU and depth (up to a few hundred meters depth) by randomly extracting from the empirical probability distributions determined by Gaudiosi et al. (2023). In this procedure, the depth of the seismic bedrock is not fixed in advance, except in the case that it has been determined in the original study. In the other cases, the thickness of the deeper layer and of respective  $V_s$  values are prolonged downward. The depth of the seismic bedrock and relevant  $V_s$  are thus fixed to the ones relative to the first stratum below which average  $V_s$  values remain above 800 m/s.

As a second step, the uniform hazard acceleration response spectrum on ground surface relative to an exceedance probability of 10% in 50 years was determined for the considered SHM by the Italian seismic hazard map (Meletti et al. 2006).

As a third step, seismic response relative to each of the simulated columns is computed using the linear equivalent approach by considering the Inverse Random Vibration Theory procedure (Kottke and Rathje 2013). The response spectrum at the surface of the considered column obtained in this way is used with the input response spectrum (the UHS determined in the previous step) to compute the  $Sf_*$  and  $AF_*$  values as defined in Eq. (1) and Eq. (2). Each  $Sf_*$  and  $AF_*$  value obtained in this way is considered as representative of a possible subsoil configuration compatible with the available seismic microzonation data.

## 4 Results

### 4.1 Coverage of NTC18 soil classes

Considering the approach described in the previous section, a total of 1,380,600 seismostratigraphic profiles were generated and for each of them the  $V_{s_{eq}}$  value (Table 1) was estimated. The level of coverage for the different NTC18 soil classes is shown in Fig. 2. Although the greatest concentration involves profiles confined within 100 m depth, a significant number of configurations extend to greater depths. Most of the situations refer classes B, C and E (54%, 24% and 17% of the total, respectively), with less coverage of classes A and D (4% and 0.7%, respectively), poorly represented in the seismic microzonation studies considered. There is also a small proportion of situations that do not fall into any of the categories (0.03% of the total). It is important to emphasize that this distribution reflects the distribution of seismostratigraphic situations present in the Italian territory as we know them from the seismic microzonation studies performed so far.



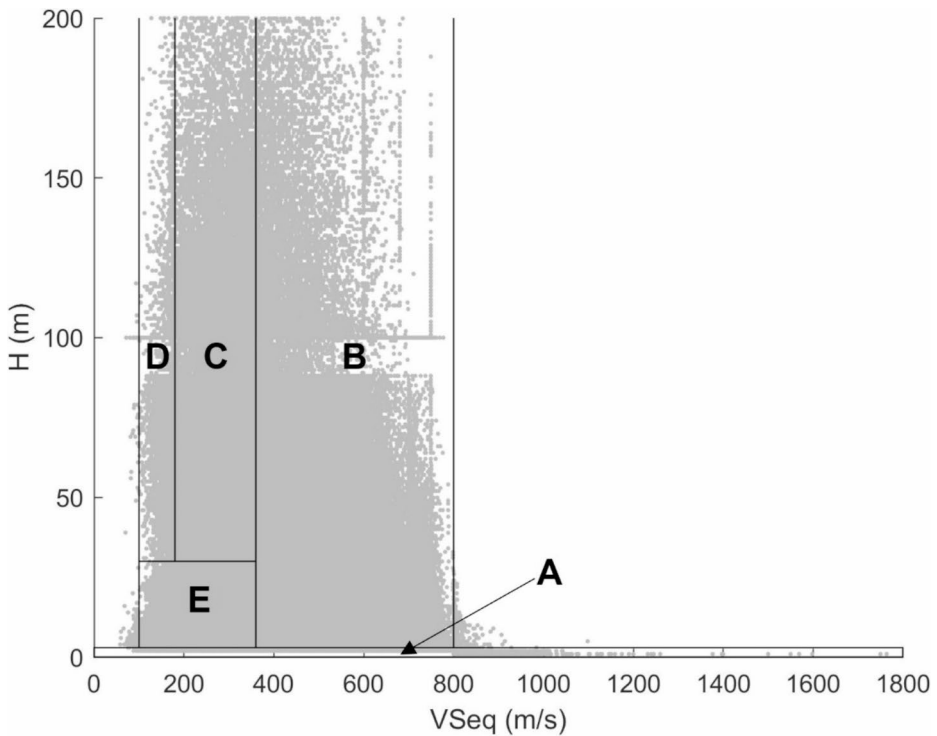


**Fig. 2** Statistical coverage of the 1,380,600 simulated profiles as a function of relative equivalent velocity value ( $V_{Seq}$ ) according to NTC18 and the seismic bedrock depth ( $H$ )

From the simulation results,  $Sf_*$  factors as a function of the vibration period were computed from the ratios between the response spectrum at the modeled column surface and the reference response spectrum for the same column for the corresponding NTC18 soil class. Median and standard deviation of  $\ln Sf_*$  values are given in Appendix 2 for the different soil classes.

#### 4.2 Median $Sf_*$ values

Figure 3 shows the population median of the  $Sf_*$  factors obtained for vibration periods between 0.01s and 2s for each soil class; these curves are grouped according to the site-related PGA value. As can be seen, the effect of the reference hazard PGA value appears to be modest, while the effect of the soil class is very clear. For classes B and E, the median value is always greater than 1 with maximum amplitudes occurring around the period of 0.3s, reaching a maximum amplitude of 1.3 for class B and 1.7 for class E. For class C, values up to 1.6 are obtained (for periods around 1s), but deamplification ( $Sf_C < 1$ ) is also observed for lower periods. For class D, both deamplification for short periods and amplification for long periods appear more pronounced. The deamplification regarding the shorter periods was indeed also observed in the case of the Kik-Net network (Paolucci et al. 2021) and does not depend directly on the limitations of the numerical approach used,

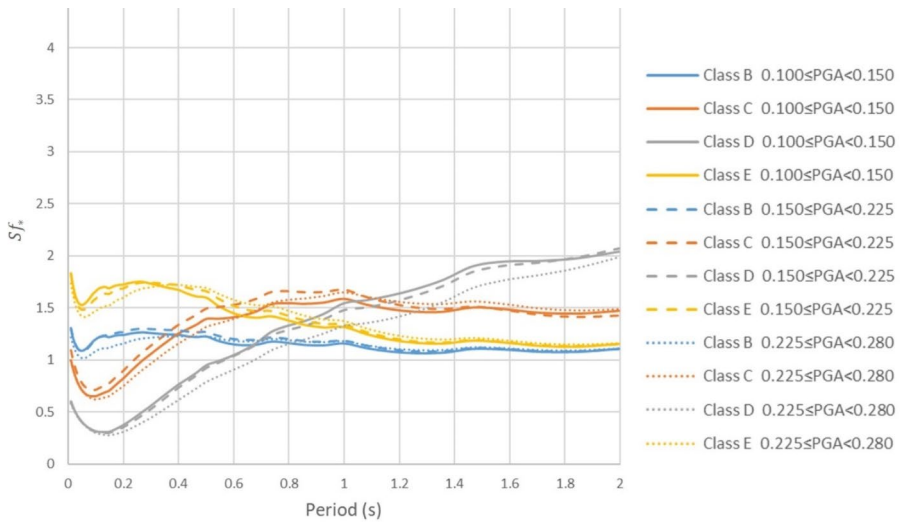


**Fig. 3** Median values of  $Sf_*$  factors obtained by numerical simulations for different soil classes for each vibration period. Solid, dotted, and dashed lines refer to the values obtained for different hazard levels (expressed in PGA classes and defined as fraction of  $g$ )

which would tend to overestimate the shaking effect for the deeper covers (Yoshida et al. 2002; Kausel and Assimaki 2002).

It is worth comparing these results with analogous ones determined considering the standardized 5% damped acceleration response spectra computed according to NTC18 simplified approach. Figure 4 shows the ratios between response spectra determined as a function of the soil class and the reference UHS (also standardized following NTC18) determined by the point grid constituting the Italian seismic hazard map. Since the spectral shape in NTC18 also depends on the geographical coordinate, only the point closest to the locations considered in the numerical analysis were considered. The greater difference between the curves referred to the different PGA classes than those shown in Fig. 3 (more evident for soil classes C, D and E) indicates that the incidence of seismic hazard is greater than that inferred from the numerical simulations for periods  $> 0.2s$ . In this range of periods, the normative values seem to provide much more conservative indications than that deduced from the numerical simulations. It is also noted that no deamplification effects are suggested for any of the soil classes.

Another way to represent the effect of the different subsoil configurations as inferred from the numerical simulations and those predicted by the regulation simplified approach is through the respective  $AF_*$  values. Figure 5 compares the populations of the  $AF_*$  values obtained in the different ranges of vibration periods as determined by Eq. (2). As concerns  $AF_*$  for NTC18 response spectra ( $AF_{*,NTC18}$ ), these values were computed by Pergalani et al. (2020) for all the Italian municipalities: in this case, only  $AF_{*,NTC18}$  values of the locations considered in the numerical analysis were used.

The distribution of the differences ( $Diff = AF_{*,NTC18} - AF_{*,simulated}$ ) related to the different soil classes are shown in Fig. 6. For the shorter periods (0.1–0.5 s), the median of the differences related to class B is very close to zero, suggesting the values that the respec-

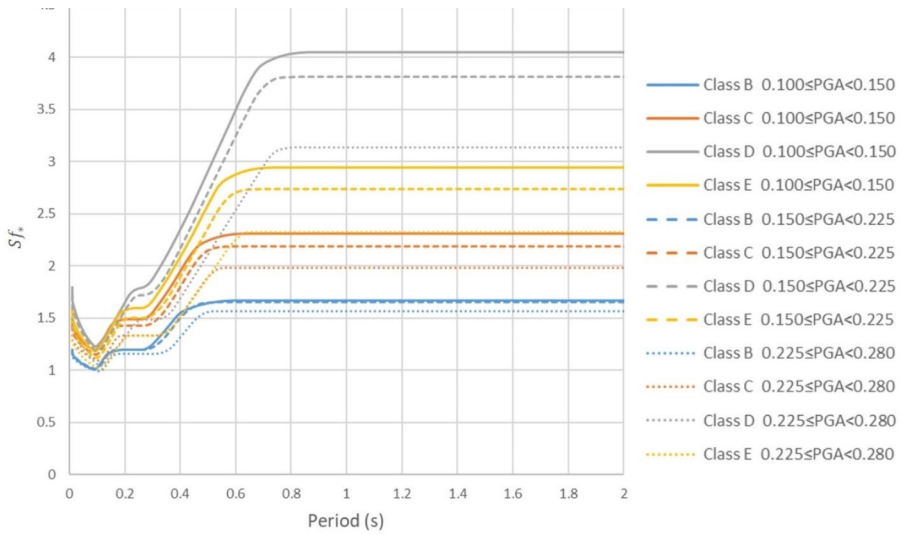


**Fig. 4** Trend of median values of  $S_f^*$  factors obtained by following the provisions of the NTC18 simplified approach. The solid and dashed lines refer to the values obtained for the different hazard levels (expressed in PGA classes and defined as fraction of  $g$ ) at the sites considered for the numerical simulation

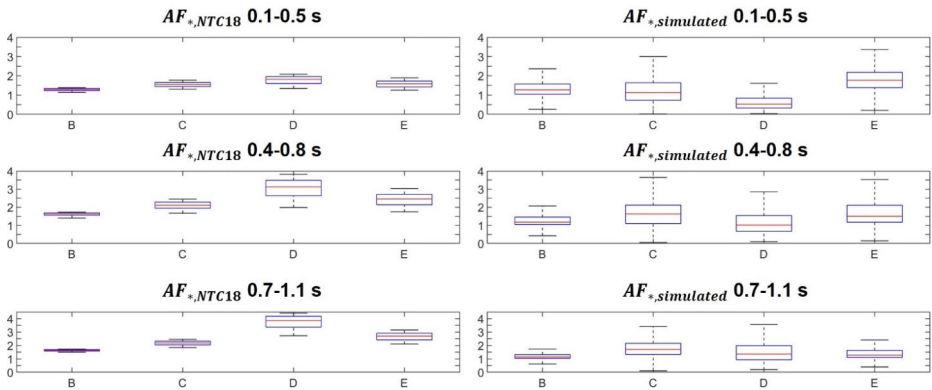


**Fig. 5** Distribution of Amplification Factors (Eq. 2) related to the different soil classes and for the three vibration period intervals (0.1–0.5 s, 0.4–0.8 s and 0.7–1.1 s). On the left are the values obtained by applying NTC18 simplified approach ( $AF_{*,NTC18}$ ) and on the right are those obtained by numerical simulations using seismic microzonation data ( $AF_{*,simulated}$ ). On each box, the central red mark indicates the median, and the bottom and top edges of the blue box indicate the 25th and 75th percentiles, respectively; the whiskers extend to the most extreme data points not considered outliers

tive mean values are close; similar result occurs for class E, with a slight underestimate of the median value by NTC18. In contrast, as concerns other soil classes and longer periods, the normative values tend to predict higher average amplification values than those inferred from numerical simulations.

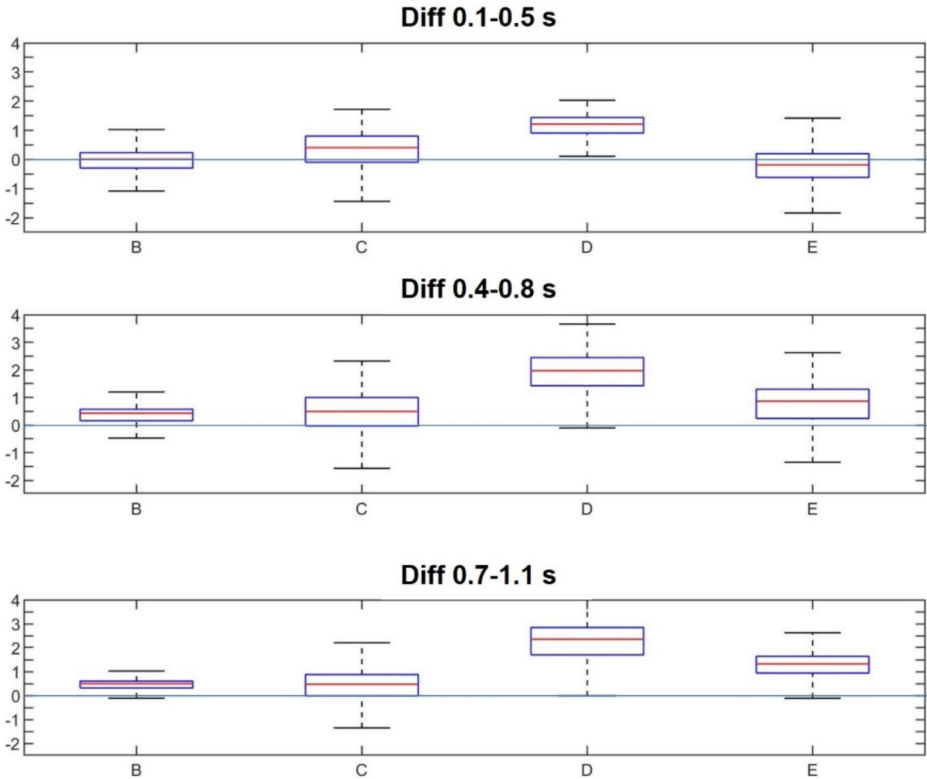


**Fig. 6** Distribution of differences (Diff) between the amplification factors of the normative and those obtained from numerical simulations for different soil classes for the three vibration period intervals. Values greater than zero (blue solid line) indicate that the normative values are greater than those deduced from the numerical simulations. On each box, the central red mark indicates the median, and the bottom and top edges of the blue box indicate the 25th and 75th percentiles, respectively; the whiskers extend to the most extreme data points not considered outliers

### 4.3 Variability of $Sf_*$ values

In order to evaluate  $Sa_*$  from Eq. (8), the respective importance of the terms  $\sigma_{\ln Sa_A}^2$  and  $\sigma_{\ln Sf_*}^2$  should be evaluated. The values of  $\sigma_{\ln Sa_A}$  relative to different vibration periods can be computed at the considered sites from the respective UHS. In practice, the parameters  $\mu_{\ln Sa_A}$  and  $\sigma_{\ln Sa_A}$  of the log-normal distributions representative to the local reference hazard are obtained by best fitting the exceedance probabilities relative to an exposure period of 50 years characterized by the return periods reported in the reference hazard map. An example of this procedure is reported in Appendix 1 relative to the city of L'Aquila in Central Italy, where the considered return periods are shown in Table 2A. The distribution of the  $\sigma_{\ln Sa_A}$  values obtained in this way for all the sites considered in the numerical simulations is summarized in Fig. 7a.

The distribution of  $\sigma_{\ln Sf_*}$  values obtained from numerical simulations relative to each soil classes are reported in Fig. 7b (the same values are listed in Appendix 2).

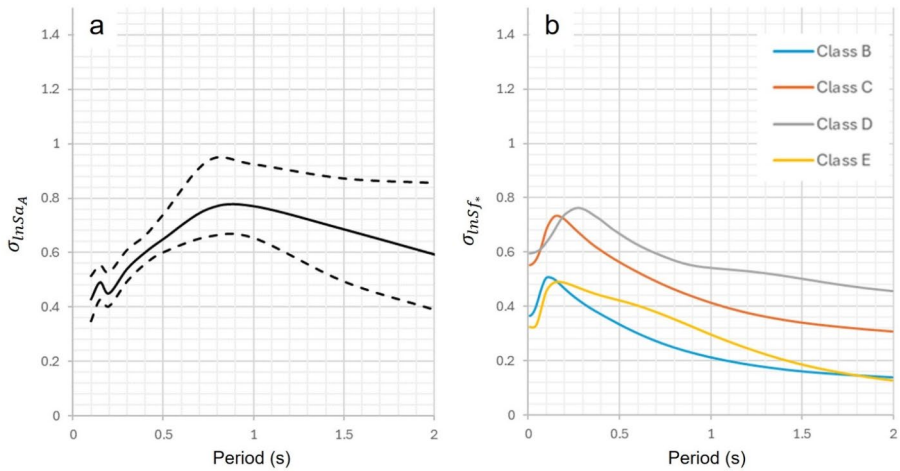


**Fig. 7** Standard deviations ( $\sigma$ ) of  $\ln Sa_A$  values associated with different hazard estimates according to Eq. (4) for different vibration periods for the considered sites (a) and of  $\ln Sf_*$  values (Eq. (5)) obtained in numerical simulations (b). As concerns the  $\sigma_{\ln Sa_A}$  values, solid line indicates the median of the values inferred by the reference hazard map; dashed lines indicate the bounds of the interquartile range

In general, it is possible to note that the values of  $\sigma_{\ln Sa_A}$  and  $\sigma_{\ln Sf_*}$  have about the same order of magnitude: therefore, the latter cannot be considered negligible. One can see that variability of  $\ln Sf_*$  values is larger for soil classes C and D, possibly due to the large variations expected in the depth of engineering bedrock for these classes. In general, a larger variability characterizes short periods in all the subsoil classes. This is the possible effect of the marked variability of the Vs values expected at shallow depths.

More in general, in Fig. 8, the trends of  $Sf_*$  values showed in Fig. 3 are compared with those in NTC18 (Fig. 4) and those obtained using the site-specific factors for NTC18 proposed by Andreotti et al. (2018): in the latter case, the 84th percentile of the distribution of the site factors obtained from their numerical simulations is considered (Table 4 of Andreotti et al. 2018). As one can see, the levels of variability shown in the population of values obtained from the numerical simulations described above (black curves) are very wide, especially for classes C, D, and E. In class C and class B there is good agreement with the 84th percentile of the estimates provided from this study and those obtained by Andreotti et al. (2018) (blue curves), at least for periods lower than 1s. Greater differences between these authors and this study appear for classes D and E, especially for vibration periods longer than 1s. These differences may be related to the greater extension of the case histories considered in the simulations performed within the framework of this project compared to what Andreotti et al. (2018) produced, but also (regarding class D) to the reduced number of cases examined in the present study compared to those in the other classes. As concerns the comparison with NTC18 (red curves), the latter estimates appear very similar to the median of  $Sf_*$  from this study for class B and for periods lower than 0.4 s; instead, for the same period interval, a significant underestimation can be observed for class E and, as for class B, an evident overestimation for the period higher than 1s occurs. For class C and D, NTC18 estimates are characterized by a similar trend to that of Andreotti et al.

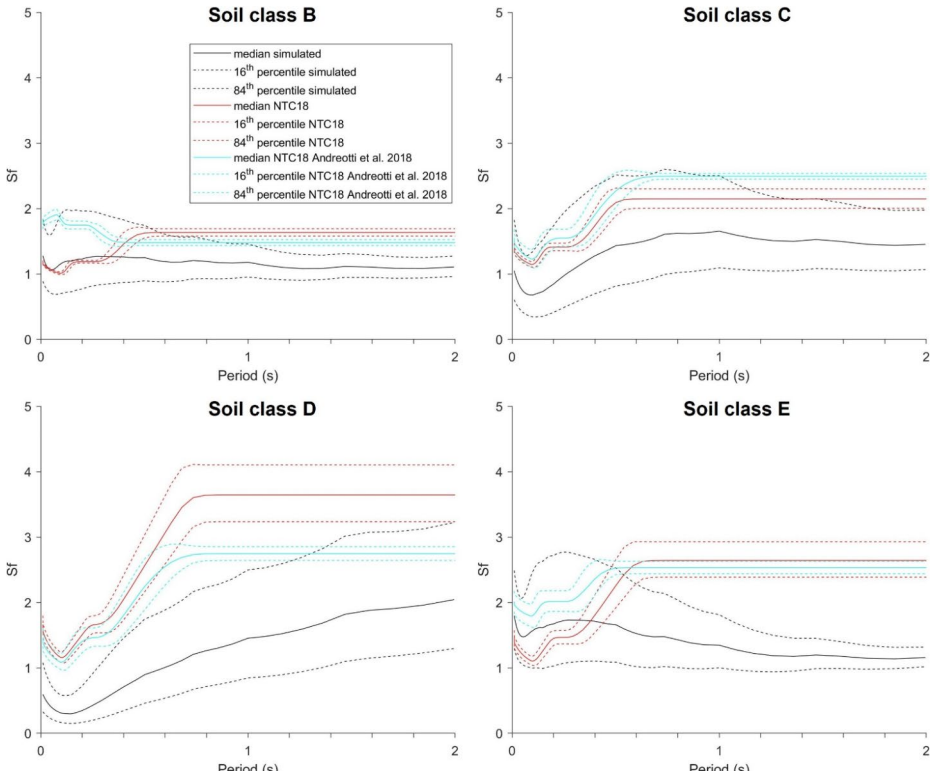


**Fig. 8** Comparison of  $Sf_*$  estimates for different soil classes and vibration periods according to the NTC18 standard (in red), the estimates of Andreotti et al. (2018) (in blue), and those obtained from numerical simulations based on data of seismic microzonation studies carried out in Italy (in black)

(2018). To estimate the impact of  $Sf_*$  variability, an approximate approach can be used. First, given the lower sensitivity of the amplification estimates to the level of reference hazards, the covariance term in Eq. (8) could be considered negligible in a first approximation. One could then state that

$$\ln Sa_*(\alpha) \cong \mu_{\ln Sa_A} + \mu_{\ln Sf_*} + k \sqrt{\sigma_{\ln Sf_*}^2 + \sigma_{\ln Sa_A}^2} \tag{12}$$

If we also consider that  $\sigma_{\ln Sa_A} \cong \sigma_{\ln Sf_*}$ , in a first approximation, the relationship could be simplified to the form

$$\ln Sa_*(\alpha) \cong \mu_{\ln Sa_A} + \mu_{\ln Sf_*} + k \sigma_{\ln Sa_A} (\sqrt{2}) \tag{13}$$

In the case of current practice in which the  $Sf_*$  factor is included without including its relative variance, we would have

$$\ln Sa'_*(\alpha) \cong \mu_{\ln Sa_A} + k\sigma_{\ln Sa_A} + \mu_{\ln Sf_*} \tag{14}$$

i.e.,

$$\ln Sa_*(\alpha) \cong \ln Sa'_*(\alpha) + k\sigma_{\ln Sa_A}(\sqrt{2} - 1) > \ln Sa'_*(\alpha), \tag{15}$$

showing how current practice tends to underestimate the effect of site conditions by a factor proportional to a fraction of  $\sigma_{\ln Sa_A}$ .

The possible impact of outcomes described above on the response spectra relative to different soil classes ( $Sa_*$ ) can put in evidence by considering the case of the city of L'Aquila in Central Italy. This town is located in a high hazard area and was severely damaged by the seismic sequence that stroke Central Italy in 2009 (e.g., Ameri et al. 2011). In Fig. 9, the spectra computed by considering  $\ln Sf_*$  values deduced by our simulations and implemented with their uncertainties in Eq. (12) on UHS (relative to an exceedance probability of 10% in 50 y) are compared with the spectra provided by following NTC18. One can see, that as concerns the period range of main interest for common building (<0.5 s), NTC18 estimates appear generally less conservative than the ones obtained by our simulations, except as concerns subsoil class D. This underestimate appears particularly severe for soil class E. For longer periods instead, NTC18 provides conservative (extremely conservative in the case of class E) values.

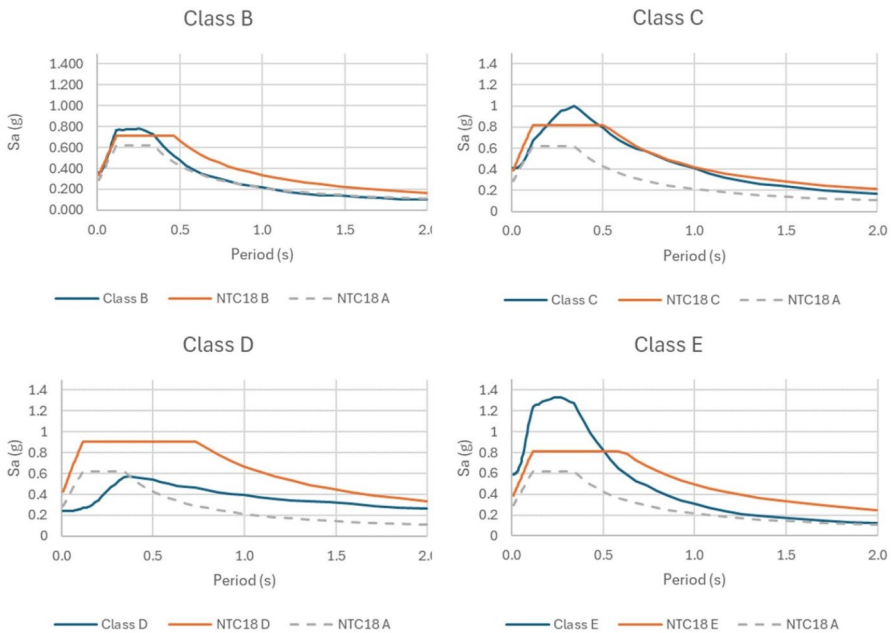


**Fig. 9** Response spectra deduced for the NTC18 soil classes at city of L'Aquila (Central Italy) by considering the approach presently adopted in the norm (brown line) and the one here proposed (blue line). Soil class A response spectrum relative to an exceedance probability of 10% in 50 y ([https://esse1-gis.mi.ingv.it/mps04\\_eng.jsp](https://esse1-gis.mi.ingv.it/mps04_eng.jsp)) is also reported for reference (dashed gray line)

#### 4.4 Comparison with estimates from the empirical approach

As stated above, accelerometric data can be used to constrain  $Sf_*$  values by adopting a statistical approach (Paolucci et al. 2021 and references therein) have been considered. Outcomes of this approach (the so-called site amplification functions “ $\delta S2S$ ”; Al-Atik et al. 2010) to accelerometric sites in the Italian area are reported by Lanzano et al. (2024a) and have been compared with estimates provided in the present study. To this purpose, the set of comparison situations was selected by considering sites classified by following NTC18 on the basis of an experimental  $V_s$  profile at the accelerometric site. As a whole, 254 sites were selected and among them: 21 are of class A, 147 of class B, 65 of class C, 5 of class D and 16 of class E. As one can see, only soil classes B and C are characterized by a significant set of data: for this reason, it has been considered appropriate to take into account only these two classes for the comparison with the outcomes of the numerical simulations. The distribution of estimated  $Sf_*$  values for sites belonging to the same soil class has been considered to evaluate the median  $Sf_*$  and the range of variation for each period (Fig. 10). As concerns class B, one can see a good agreement between the two estimates; however, a systematic misfit exists regarding soil class C. In particular, empirical estimates provide  $Sf_*$  values more conservative than those from numerical simulations for the whole range of periods. Beyond the large variability which characterizes both data sets, this discrepancy should be considered as significant. A main difference between the two approaches relies on the role of nonlinear behavior of subsoil materials, which is considered in numerical simulations and disregarded in empirical evaluations (e.g., Paolucci et al. 2021). In fact, most of accelerometric data only concerns relatively weak motions, generally well below the threshold (of the order of 0.1 g) for the activation of nonlinear effects (e.g., Kaklamanos et al. 2013 and 2015); this can be verified consulting the metadata of the waveform dataset (Lanzano et al. 2024b) used for the analysis based on the empirical data. In this regard, one should note that the observed systematic bias mainly concerns deep soft soils which are generally characterized by high strain values during strong earthquakes. On the other hand, due to the lack of experimental data about mechanical properties of deep-seated sediments may provide biased results. Moreover, one should consider that nonlinear effects are expected

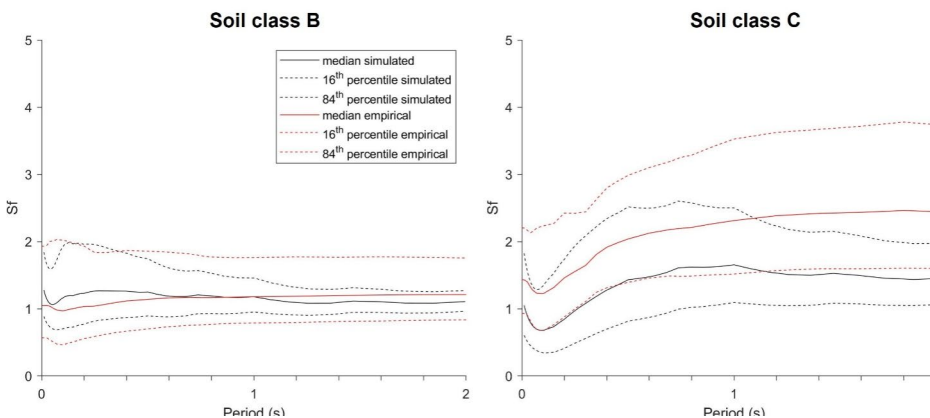


**Fig. 10** Comparison of  $Sf_*$  values obtained by the empirical approach (red curves) and numerical simulations (black curves) relative to soil class B and C



to mainly concern periods below 0.5 s (Kaklamanos et al. 2013). Thus, the extension of the considered bias between empirical and simulated values over the whole range of periods cannot be explained on this basis.

Another main difference between the two considered approach is that, while in numerical simulations 1D conditions are strictly respected, in the empirical approach eventual 2D-3D effects due to lateral variations on the subsoil conditions are included by violating the prescriptions of the considered seismic code. Probably, strict 1D conditions does not exist, in particular when long period waves are considered (Stewart et al. 2014): this may be a limitation of the Italian norm.

### 5 Discussion and conclusions

The results of numerical modeling carried out from the data provided by seismic microzonation studies seem to indicate that the ways in which NTC18 intends to account for local seismo-stratigraphical conditions may underestimate the expected effects with respect to ground motion amplification for short periods and largely overestimate them for longer periods.

Regarding the first aspect, the effect is certainly related to the underestimation of the possible impact on the expected shaking of the variability of the expected amplification effects for different soil classes.

To overcome the problem, two solutions are possible. The first is implementing site factors within the GMPEs and developing hazard maps specific for each subsoil class. This could avoid the possible biases by allowing to consistently handle the uncertainties including those related to stratigraphical 1D site effects. Alternatively, to preserve the current approach and maintain some formal consistency with the probabilistic treatment, following the suggestion of Andreotti et al. (2018), we propose to compute the spectral ordinates values ( $Sa''_*$ ) for any soil class different from the reference one, by the formula

$$\ln Sa''_* = \ln Sa'_*(\alpha) + r\sigma_{\ln Sf_*}, \tag{16}$$

where  $r$  is assumed to be 1, i.e., by considering the 84th percentile of the population of  $\ln Sf_*$  values obtained from simulations. However, this choice results in the overestimate of the spectral ordinates. In fact, the term  $r$  should be chosen to provide the same results of Eq. (8) when the covariance term is neglected. To this purpose, one should have

$$k\sqrt{\sigma_{\ln Sf_*}^2 + \sigma_{\ln Sa_A}^2} \cong r\sigma_{\ln Sf_*} + k\sigma_{\ln Sa_A} \tag{17}$$

i.e.,

$$r \cong k \frac{\sqrt{\sigma_{\ln Sf_*}^2 + \sigma_{\ln Sa_A}^2} - \sigma_{\ln Sa_A}}{\sigma_{\ln Sf_*}} \tag{18}$$

If we assume that  $\sigma_{\ln Sa_A} \cong \sigma_{\ln Sf_*} = \sigma$ ,

$$r \cong k \left( \sqrt{2} - 1 \right) \cong 0.4k \tag{19}$$

when  $k=1.28$  ( $\alpha=0.1$ ) then  $r$  is about 0.7, which corresponds to the 67th percentile of the probability distribution of the  $\ln Sf_*$ , lower than the one proposed by Andreotti et al. (2018).

The apparent overestimation of amplification proposed by the code for longer vibration periods deserves some specific consideration. This effect cannot be due to inherent limitations of the procedure used for numerical simulations (Yoshida et al. 2002; Kausel and Assimaki 2002): in fact, those approximations should produce possible overestimates of the amplification but only for the shorter periods and soft deep deposits (class D). Another possibility could be related to the insufficiency of 1D modeling for long periods where 2D/3D effects and the role of seismic phases related to surface waves could prove to be very significant. Regarding the latter point, however, it should be noted that the simplified approach of the code should not be applied where these effects are assumed to exist. A possible and more plausible explanation could be provided by the fact that the numerical simulations were based on the UHS deduced from the seismic hazard model and not on the regularized UHS. Figure 11 shows the ratios between the amplitudes of the UHS of the hazard model and the regularized UHS relative to a return period of 475 years for the same locations. While this ratio is close to 1 for periods between 0.1 and 0.5, the regularized spectrum systematically overestimates the UHS spectrum for periods greater than 0.5. This inconsistency between the regularized spectrum and that of the hazard model may be even greater for the UHS spectrum possibly calculated for different soil classes, and this may explain at least part of the observed discrepancies.

The comparison between with empirical and simulated  $Sf_*$  estimates suggests that as concerns soil class C, significant discrepancies exist and could be at least partially explained with the main methodological assumptions behind both approaches. Anyway, this prevents

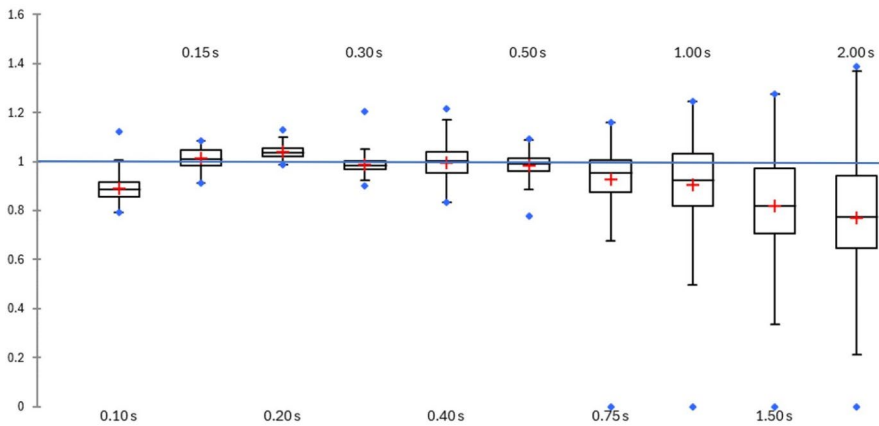


**Fig. 11** Distributions of the amplitude ratios of the uniform probability response spectra from the hazard model and those according to NTC18 for the reference subsurface versus different vibration periods in seconds. Values less than 1 indicate that the regularized spectra overestimate those of the hazard model. On each box of the chart on the right, the central black line indicates the median, the red cross represents the mean, and the bottom and top edges of the box indicate the 25th and 75th percentiles, respectively; the whiskers extend to the data point whose value is lower than 1.5 times the interquartile range from the bottom of top of the box; the data points exceeding this limit are the outliers of the distributions (blue dots)

any possibility of a mutual validation of the estimates and leaves inconclusive (now) any attempt in this direction.

In conclusion, the analyses described in the paper, rather than proposing the  $Sf_*$  values obtained by numerical simulations within the code in place of existing ones, suggest that a general rethinking of the procedures from the current regulations is desirable to consider local stratigraphic conditions and their uncertainties relative to the simplified approach. In particular, it was pointed out that the current approach may significantly underestimate amplification effects for periods below 0.5s and even more significantly overestimate those for longer periods. Several approaches exist to remedy these problems (one was proposed in the text) but all have limitations that should be discussed but seeking maximum consistency with the overall probabilistic character of the approach of the national seismic code.

### Appendix 1

The Table 2 shows the hazard data relative to the reference soil condition at the city of L'Aquila (Central Italy) as reported in the Italian seismic hazard model (Meletti et al. 2006). In the assumption that the hazard curve  $P(>PGA)$  can be represented as a log-normal distribution with average  $\mu_{\ln PGA}$  and standard deviation  $s_{\ln PGA}$ , one has

$$\ln PGA(P) = \mu_{\ln PGA} + k(P) \sigma_{\ln PGA}$$

The values of  $\mu_{\ln PGA}$  and  $s_{\ln PGA}$  can be inferred by best fitting the  $\ln PGA$  values in the Table 2 and result to be -2.07 and 0.59 respectively. The estimated values of  $\ln PGA^*$  Eq. (4) are reported in the Table. The maximum discrepancy between the reference and estimated values in PGA are always less than 6% of the reference value.

**Table 2** A Hazard estimates for the city of L'Aquila. For each return period (T in years) and exceedance probability P, the natural logarithm of the PGA value ( $\ln PGA$ ) is reported

T	P	k	$\ln PGA$ (g)	$\ln PGA^*$ (g)
30	0.811	-0.88	-2.54	-2.60
50	0.632	-0.34	-2.26	-2.27
72	0.501	0.00	-2.10	-2.08
100	0.393	0.27	-1.95	-1.91
140	0.300	0.52	-1.81	-1.76
475	0.100	1.28	-1.34	-1.31
1000	0.049	1.66	-1.10	-1.09
2500	0.020	2.06	-0.79	-0.85

Column k reports the fraction of standard deviations corresponding to the P value relative to a normal distribution. In the last column, the  $\ln PGA^*$  values estimated in the assumption that the hazard curve can be represented as a log-normal distribution are reported

## Appendix 2

Median ( $\mu_{\ln Sf_*}$ ) and standard deviation ( $\sigma_{\ln Sf_*}$ ) of the logarithm of soil factors  $Sf_*$  (Eq. 1) for different vibration periods deduced from numerical simulations performed from Italian seismic microzonation data.

Period (s)	Class B		Class C		Class D		Class E	
	$\mu_{\ln Sf}$	$\sigma_{\ln Sf}$	$\mu_{\ln Sf}$	$\sigma_{\ln Sf}$	$\mu_{\ln Sf}$	$\sigma_{\ln Sf}$	$\mu_{\ln Sf}$	$\sigma_{\ln Sf}$
0.010	0.246	0.365	0.050	0.552	-0.519	0.595	0.588	0.325
0.011	0.239	0.366	0.040	0.552	-0.529	0.595	0.580	0.324
0.012	0.230	0.366	0.030	0.552	-0.539	0.595	0.571	0.324
0.013	0.222	0.366	0.019	0.553	-0.550	0.595	0.562	0.324
0.014	0.213	0.366	0.008	0.553	-0.562	0.595	0.552	0.324
0.015	0.203	0.367	-0.005	0.553	-0.575	0.595	0.542	0.324
0.016	0.193	0.367	-0.018	0.553	-0.589	0.596	0.532	0.324
0.017	0.183	0.368	-0.031	0.554	-0.603	0.596	0.521	0.324
0.018	0.172	0.368	-0.046	0.554	-0.619	0.596	0.510	0.324
0.020	0.161	0.369	-0.061	0.555	-0.635	0.596	0.498	0.323
0.022	0.151	0.370	-0.077	0.555	-0.652	0.596	0.487	0.323
0.023	0.140	0.372	-0.094	0.556	-0.670	0.597	0.475	0.323
0.025	0.129	0.373	-0.112	0.557	-0.689	0.597	0.463	0.323
0.027	0.118	0.375	-0.130	0.558	-0.710	0.597	0.452	0.323
0.029	0.107	0.377	-0.149	0.559	-0.731	0.597	0.440	0.323
0.032	0.097	0.380	-0.168	0.561	-0.753	0.598	0.429	0.323
0.034	0.088	0.384	-0.188	0.563	-0.777	0.598	0.419	0.324
0.037	0.080	0.388	-0.209	0.565	-0.802	0.599	0.410	0.325
0.040	0.073	0.392	-0.229	0.568	-0.827	0.600	0.402	0.327
0.043	0.067	0.398	-0.250	0.571	-0.854	0.600	0.396	0.329
0.046	0.063	0.405	-0.271	0.575	-0.882	0.601	0.391	0.333
0.050	0.061	0.412	-0.291	0.580	-0.911	0.602	0.389	0.339
0.054	0.061	0.421	-0.310	0.585	-0.940	0.604	0.388	0.346
0.058	0.065	0.431	-0.328	0.592	-0.970	0.606	0.389	0.355
0.063	0.070	0.442	-0.345	0.600	-1.001	0.608	0.393	0.366
0.068	0.079	0.454	-0.360	0.610	-1.032	0.610	0.399	0.379
0.074	0.091	0.465	-0.371	0.621	-1.063	0.614	0.408	0.393
0.079	0.105	0.477	-0.380	0.635	-1.093	0.618	0.418	0.408
0.086	0.121	0.488	-0.385	0.650	-1.123	0.623	0.430	0.425
0.093	0.138	0.498	-0.387	0.666	-1.153	0.629	0.442	0.441
0.100	0.150	0.505	-0.388	0.682	-1.181	0.636	0.450	0.455
0.108	0.164	0.507	-0.375	0.695	-1.192	0.642	0.464	0.464
0.117	0.172	0.507	-0.362	0.707	-1.201	0.651	0.472	0.472
0.126	0.178	0.506	-0.347	0.717	-1.209	0.660	0.477	0.479
0.136	0.181	0.503	-0.332	0.726	-1.213	0.670	0.480	0.484
0.147	0.178	0.498	-0.317	0.732	-1.214	0.683	0.478	0.488
0.158	0.187	0.492	-0.284	0.734	-1.189	0.697	0.488	0.490
0.171	0.198	0.484	-0.245	0.732	-1.151	0.711	0.501	0.490
0.185	0.205	0.475	-0.207	0.728	-1.107	0.725	0.509	0.489
0.200	0.207	0.466	-0.170	0.721	-1.059	0.738	0.513	0.486
0.215	0.218	0.456	-0.121	0.712	-0.994	0.746	0.526	0.483

	Class B	Class C	Class D	Class E				
0.233	0.227	0.446	-0.073	0.701	-0.923	0.753	0.536	0.479
0.251	0.234	0.436	-0.025	0.688	-0.848	0.760	0.544	0.475
0.271	0.238	0.426	0.021	0.676	-0.770	0.763	0.549	0.469
0.293	0.236	0.415	0.063	0.663	-0.692	0.761	0.548	0.464
0.316	0.236	0.405	0.108	0.649	-0.607	0.755	0.547	0.458
0.341	0.234	0.394	0.153	0.634	-0.519	0.745	0.546	0.452
0.369	0.233	0.383	0.198	0.621	-0.432	0.732	0.543	0.446
0.398	0.232	0.372	0.243	0.607	-0.347	0.719	0.539	0.440
0.430	0.225	0.360	0.279	0.592	-0.271	0.702	0.526	0.434
0.464	0.220	0.347	0.317	0.578	-0.194	0.684	0.513	0.428
0.501	0.223	0.334	0.360	0.563	-0.111	0.667	0.506	0.422
0.541	0.197	0.320	0.370	0.548	-0.062	0.650	0.467	0.415
0.584	0.176	0.306	0.383	0.532	-0.012	0.633	0.432	0.406
0.631	0.166	0.292	0.402	0.516	0.044	0.616	0.404	0.396
0.681	0.168	0.278	0.431	0.499	0.108	0.601	0.388	0.384
0.736	0.187	0.264	0.474	0.482	0.187	0.586	0.390	0.370
0.794	0.176	0.250	0.483	0.465	0.231	0.570	0.360	0.355
0.858	0.160	0.237	0.481	0.448	0.266	0.557	0.325	0.337
0.926	0.155	0.225	0.487	0.431	0.312	0.547	0.303	0.318
1.000	0.164	0.213	0.503	0.414	0.374	0.542	0.298	0.297
1.080	0.126	0.202	0.467	0.398	0.391	0.537	0.244	0.276
1.166	0.096	0.191	0.434	0.382	0.421	0.532	0.200	0.255
1.259	0.079	0.181	0.411	0.368	0.464	0.525	0.171	0.233
1.359	0.080	0.172	0.404	0.355	0.521	0.516	0.161	0.213
1.468	0.108	0.164	0.423	0.344	0.598	0.505	0.180	0.192
1.585	0.100	0.156	0.404	0.333	0.631	0.492	0.163	0.174
1.711	0.082	0.150	0.374	0.324	0.646	0.479	0.137	0.157
1.848	0.080	0.145	0.362	0.316	0.673	0.467	0.129	0.142
1.995	0.101	0.139	0.373	0.308	0.715	0.456	0.146	0.129

**Acknowledgements** Many thanks are due to the two anonymous referees whose suggestions helped us to significantly improve the original manuscript.

**Author contributions** Both authors contributed to the study conceptualization, methodology and analysis. Data collection and curation were performed by Enrico Paolucci. Dario Albarello wrote the original draft, Enrico Paolucci did the revision and editing; both authors read and approved the final manuscript.

**Funding** This work was carried out in the framework of the project “Convenzione DPC-ReLuis 2019–2021, WP18: COntributi Normativi relativi ad Azione Sismica (CONpAS)”. Open access funding provided by Alma Mater Studiorum - Università di Bologna within the CRUI-CARE Agreement.

**Data availability** Data concerning the Italian seismic microzonation studies are available at <https://www.webms.it/>. Data concerning the Italian Seismic Hazard Map are available at [https://esse1-gis.mi.ingv.it/mps04\\_eng.jsp](https://esse1-gis.mi.ingv.it/mps04_eng.jsp). Other data will be made available on request.

## Declarations

**Competing interests** The authors declare that they have no known competing financial interests or personal relationships that could have appeared to influence the work reported in this paper.

**Open Access** This article is licensed under a Creative Commons Attribution 4.0 International License,

which permits use, sharing, adaptation, distribution and reproduction in any medium or format, as long as you give appropriate credit to the original author(s) and the source, provide a link to the Creative Commons licence, and indicate if changes were made. The images or other third party material in this article are included in the article's Creative Commons licence, unless indicated otherwise in a credit line to the material. If material is not included in the article's Creative Commons licence and your intended use is not permitted by statutory regulation or exceeds the permitted use, you will need to obtain permission directly from the copyright holder. To view a copy of this licence, visit <http://creativecommons.org/licenses/by/4.0/>.

## References

- Acunzo G, Falcone G, Lernia A, Mori F, Mendicelli A, Naso G, Albarello D, Moscatelli M (2024) NC92Soil: a computer code for deterministic and stochastic 1D equivalent linear seismic site response analyses. *Comput Geotech* 165(January 2024):105857. <https://doi.org/10.1016/j.compgeo.2023.105857>
- Aimar M, Ciancimino A, Foti S (2020) An assessment of the NTC18 stratigraphic seismic amplification factors. *RIG*, 1/2020, 5–20, <https://doi.org/10.19199/2020.1.0557-1405.005>
- Al Atik L, Abrahamson N, Bommer JJ, Scherbaum F, Cotton F, Kuehn N (2010) The variability of ground-motion prediction models and its components. *Seismol Res Lett* 81(5):794–801. <https://doi.org/10.1785/gssrl.81.5.794>
- Albarello D (2017) Extensive application of seismic microzoning: methodological and socio-political issues in the Italian experience. *Boll Geofis Teor Appl* 58(4):253–264. <https://doi.org/10.4430/bgta0205>
- Ameri G, Bindi D, Pacor F, Galadini F (2011) The 2009 April 6, mw 6.3, L'Aquila (central Italy) earthquake: finite-fault effects on intensity data. *Geophys J Int* 186(2):837–851. <https://doi.org/10.1111/j.1365-246X.2011.05069.x>
- Andreotti G, Calvi GM (2021) Nonlinear soil effects on observed and simulated response spectra. *Earthq Eng Struct Dyn* 50:3831–3854. <https://doi.org/10.1002/eqe.3535>
- Andreotti G, Famà A, Lai CG (2018) Hazard-dependent soil factors for site-specific elastic acceleration response spectra of Italian and European seismic building codes. *Bull Earthq Engg* 16:5769–5800. <https://doi.org/10.1007/s10518-018-0422-9>
- Gaudiosi I, Romagnoli G, Albarello D, Fortunato C, Imprescia P, Stigliano F, Moscatelli M (2023) G/G 0 ( $\gamma$ ) and D( $\gamma$ ) curves joined with engineering geological units in Italy. *Sci Data* 10(1):625. <https://doi.org/10.1038/s41597-023-02412-8>
- Kaklamanos J, Bradley BB, Thompson EM, Baise LG (2013) Critical parameters affecting bias and variability in site-response analyses using KiK-net downhole array data. *Bull Seismol Soc Am* 103(3):1733–1749. <https://doi.org/10.1785/0120120166>
- Kaklamanos J, Baise LG, Thompson EM, Dorfmann L (2015) Comparison of 1D linear, equivalent-linear, and nonlinear site response models at six KiK-net validation sites. *Soil Dyn Earthq Eng* 69:207–219. <https://doi.org/10.1016/j.soildyn.2014.10.016>
- Kausel E, Assimaki D (2002) Seismic simulation of inelastic soils via frequency-dependent moduli and damping. *J Eng Mech* 128(1):34–47. [https://doi.org/10.1061/\(ASCE\)0733-9399\(2002\)128:1\(34\)](https://doi.org/10.1061/(ASCE)0733-9399(2002)128:1(34))
- Kottke A, Rathje E (2008) Technical manual for strata. Report No.: 2008/10. Pacific earthquake engineering research center. Berkeley: University of California. <https://github.com/arkottke/strata/>
- Kottke AR, Rathje EM (2013) Comparison of time series and random-vibration theory site-response methods. *Bull Seismol Soc Am* 103:2111–2127. <https://doi.org/10.1785/0120120254>
- Kramer SL (1996) *Geotechnical earthquake engineering*. Prentice Hall, New Jersey, NJ, USA
- Lanzano G, Brunelli G, Sgobba S, Felicetta C, Pacor F, Mascandola C, Russo E, Luzi L (2024a) ITACAs2s flatfile 2.0: table of empirical amplification functions of the Italian recording stations. [https://doi.org/10.13127/itaca.4.0/itacas2s\\_flatfile.2.0](https://doi.org/10.13127/itaca.4.0/itacas2s_flatfile.2.0). Istituto Nazionale di Geofisica e Vulcanologia (INGV)
- Lanzano G, Vitranò L, Felicetta C, Russo E, D'Amico M, Mascandola C, Sgobba S, Brunelli G, Ramadan F, Pacor F, Luzi L (2024b) ITACAext flatfiles: parametric tables of metadata and strong motion intensity measures. Istituto Nazionale Di Geofisica E Vulcanologia (INGV). [https://doi.org/10.13127/itaca.4.0/itacaext\\_flatfile.2.0](https://doi.org/10.13127/itaca.4.0/itacaext_flatfile.2.0)
- Meletti C, Montalò V, Stucchi M, Martinelli F (2006) Database della pericolosità sismica MPS04. Istituto Nazionale Di Geofisica E Vulcanologia (INGV). <https://doi.org/10.13127/SH/MPS04/DB>. Data available at [https://esse1-gis.mi.ingv.it/mps04\\_eng.jsp](https://esse1-gis.mi.ingv.it/mps04_eng.jsp)
- Moscatelli M, Albarello D, Scarascia Mugnozza G, Dolce M (2020) The Italian approach to seismic microzoning. *Bull Earthq Eng* 18,5425–5440. <https://doi.org/10.1007/s10518-020-00856-6>

- NTC18-Ministry of Infrastructure and Transport (2018) Technical Standards for Construction, Ministry of Infrastructure and Transport, Ministerial Decree of January 17, 2018, Ordinary Supplement to Official Gazette No. 42, Feb. 20, 2018 (in Italian)
- Paolucci R, Aimar M, Ciancimino A, Dotti M, Foti S, Lanzano G, Mattevi P, Pacor F, Vanini M (2021) Checking the site categorization criteria and amplification factors of the 2021 draft of Eurocode 8 part 1–1. *Bull Earthq Engg* 19:4199–4234. <https://doi.org/10.1007/s10518-021-01118-9>
- Pergalani F, Pagliaroli A, Bourdeau C, Compagnoni M, Lenti L, Lualdi M, Madaia C, Martino S, Razzano R, Varone C, Verrubbi V (2020) Seismic microzoning map: approaches, results and applications after the 2016–2017 Central Italy seismic sequence. *Bull Earthq Eng*, 18,5595–5629.<https://doi.org/10.1007/s10518-019-00640-1>
- Pieruccini P, Paolucci E, Fantozzi PL, Naldini D, Albarello D (2022) Developing effective subsoil reference model for seismic microzonation studies: Central Italy case studies. *Nat Haz*, 112,451–474.<https://doi.org/10.1007/s11069-021-05188-5>
- Rey J, Faccioli E, Bommer JJ (2002) Derivation of design soil coefficients (S) and response spectral shapes for Eurocode 8 using the European Strong-Motion Database. *J.Seism.*, 6: 547–555, 2002. <https://doi.org/10.1023/A:1021169715992>
- Romagnoli G, Tarquini E, Porchia A, Catalano S, Albarello D, Moscatelli M (2022) The possible use of engineering-geological qualitative characterization of shallow subsoil for a preliminary estimate of the vs profile in seismic microzonation studies. *Soil Dyn Earthq Eng* 161:107347. <https://doi.org/10.1016/j.soildyn.2022.107347>
- SM-WG (Seismic Microzonation - Working Group) (2008) Guidelines for Seismic Microzonation. Conference of Regions and Autonomous Provinces of Italy-Civil Protection Department, Rome, 3 vols. and DVD. English edition published online in 2015, <https://www.centromicrozonazioneismica.it/en/tools/guidelines-sm/>
- Stewart JP, Afshari K, Hashash YMA (2014) Guidelines for performing hazard-consistent one-dimensional ground response analysis for ground motion prediction. PEER report No. 2014/16201416. Pacific Earthquake Engineering Research Center, Berkeley, CA
- Yoshida N, Kobayashi S, Suetomi I, Miura K (2002) Equivalent linear method considering frequency dependent characteristics of stiffness and damping. *Soil Dyn Earthq Eng* 22(3):205–222. [https://doi.org/10.1016/S0267-7261\(02\)00011-8](https://doi.org/10.1016/S0267-7261(02)00011-8)

**Publisher's note** Springer Nature remains neutral with regard to jurisdictional claims in published maps and institutional affiliations.